

Charge rearrangement and screening in a quantum point contact

S. Lüscher,¹ L. S. Moore,¹ T. Rejec,² Yigal Meir,² Hadas Shtrikman,³ and D. Goldhaber-Gordon¹

¹*Department of Physics, Stanford University, Stanford, California 94305*

²*Department of Physics, Ben Gurion University of the Negev, Beersheva, Israel*

³*Submicron Center, Weizmann Institute of Science, Rehovot, Israel*

(Dated: October 12, 2018)

Compressibility measurements are performed on a quantum point contact (QPC). Screening due to mobile charges in the QPC is measured quantitatively, using a second point contact. These measurements are performed from pinch-off through the opening of the first few modes in the QPC. While the measured signal closely matches a Thomas-Fermi-Poisson prediction, deviations from the classical behavior are apparent near the openings of the different modes. Density functional calculations attribute the deviations to a combination of a diverging density of states at the opening of each one-dimensional mode and exchange interaction, which is strongest for the first mode.

PACS numbers: 73.21.Hb, 73.23.-b, 73.43.Fj, 73.61.Ey, 71.45.Gm, 73.43.Cd

The simplest of mesoscopic systems is a point contact, a narrow constriction between two electron reservoirs. Conductance measurements through such a quantum point contact (QPC) reveal steps in units of $G_0 \equiv 2e^2/h$. The physics of these steps is well understood: for a QPC adiabatically connected to the reservoirs, the transmission coefficient of each mode is either zero or one. The number of such modes increases, as the width of the QPC is increased, leading according to the Landauer formula to a series of quantized steps in conductance. Such conductance measurements, however, also reveal our limited knowledge of the physics of QPCs at low densities. As a QPC is just being opened up, its conductance pauses around $0.7 \times G_0$, before rising to the first full-channel plateau. This “0.7 structure” has been one of the prime puzzles in mesoscopic physics [1]. Longer 1D wires show a similar, and likely related, structure at $0.5 \times G_0$ [2]. These features have been variously attributed to spontaneous spin polarization in the QPC [3, 4, 5], to Luttinger liquid behavior [6], or to the formation of a localized moment at the QPC [7, 8, 9], together with the resulting Kondo effect.

To shed more light on the physics of QPCs near pinch-off, we report here measurements of the compressibility of electrons in the channel of the QPC. To measure compressibility, one applies a potential to an electrode on one side of a structure of interest, and measures the potential on the other side. Compressibility measurements have helped elucidate how charge carriers arrange themselves in two dimensions when kinetic energy is dominated by interactions, whether in the quantum Hall regime [10] or at low density and high effective mass [11]. Augmented by local electrostatic detectors, such measurements have produced striking images of how individual carriers localize in these same regimes [12]. Compressibility measurements using nanofabricated electrostatic detectors such as QPCs have also become a standard tool to probe transitions between charge states of a quantum dot or two coupled quantum dots [13, 14, 15]. In this letter we

present analogous measurements, using a QPC as an electrostatic detector but measuring in this case the charge configuration of a second QPC instead of a quantum dot, c.f. Ref. [16].

Compressibility of perfect 1D systems is a textbook problem. The diverging density of states should give strong compressibility at low carrier density. In a multi-mode 1D system, one would expect that a similar signature should occur at the opening of each mode. In contrast, both experiment and numerical simulation of our short 1D wire show that the enhancement in compressibility at the opening of the first mode is significantly different from that at the opening of higher modes. In retrospect, this might have been expected because at the opening of the first mode the total density is small and thus exchange effects are also important. In addition, the distinctive “0.7” transport feature might have had a counterpart in compressibility. As it turns out, the simulated compressibility feature associated with the 0.7 regime was too weak to observe experimentally with our current sensitivity.

The devices in this experiment were fabricated on a GaAs/AlGaAs heterostructure, containing a two-dimensional electron gas (2DEG) 70 nm below the surface. The electron density $n_s = 2 \cdot 10^{11} \text{ cm}^{-2}$ and mobility $\mu = 2.3 \cdot 10^6 \text{ cm}^2/(\text{Vs})$ at 4.2 K. A schematic of the measured devices is shown in the inset of Fig. 1(a). Two QPCs, with lithographic widths of 330 nm and 350 nm, respectively, are separated by an 80 nm wide gate. Although the device is symmetric in design, the two QPCs play fundamentally different roles in our experiment: the lefthand QPC serves as a detector, sensitive to charge rearrangements in the righthand QPC. For clarity, we will henceforth refer to the righthand QPC as “the QPC” and the lefthand QPC as “the detector.” Our data support the assumption that the primary interaction between the two QPCs is electrostatic. Two nominally-identical devices, each containing a QPC and a detector, were measured in a ^3He cryostat with 300 mK base tempera-

ture. The extensive measurements taken on one QPC-detector pair are presented in this paper; consistent behavior was also found after thermal cycling to room temperature. Measurements of another nominally-identical QPC-detector pair were used to confirm qualitative features of the data presented here.

Fig. 1(a) and (b) show the linear and non-linear differential conductance, respectively, of a QPC with the classic signatures of 0.7 structure. The charge detector signal (Fig. 1(c)) is measured as the QPC is opened from pinch-off through the third plateau. The full range of V_{qpc} is broken into 14 shorter measurements and the detector readjusted for each, to keep the detector conductance in its sensitive, near-linear regime. Each of the 14 traces in Fig. 1(c) covers a 100 mV range in V_{qpc} , with consecutive traces overlapping by 50 mV. To reduce noise we averaged each trace over 40 measurements. No striking features are visible in these raw data.

To analyze the data more carefully, we perform two transformations. First, we assign to each V_{qpc} an effective voltage, V_{eff} , that would produce the same change in the detector conductance if it were applied to the detector gate. This mapping is based on the measured response of the detector $G_{\text{det}}(V_{\text{det}})$, Fig. 1(c) inset. The result of this transformation is shown in Fig. 1(c) (right axis). Second, the derivative $D \equiv dV_{\text{eff}}/dV_{\text{qpc}}$ eliminates the offsets between consecutive traces. This quantity describes the relative coupling of the detector to V_{qpc} and V_{det} , and thus provides a quantitative measure of the screening of V_{qpc} by mobile charges in and around the QPC.

The derivatives of the 14 measurements shown in Fig. 1(c) are plotted in Fig. 1(d). The overlapping ranges of each curve agree, allowing us to extract a continuous $D(V_{\text{qpc}})$. The QPC conductance is superimposed on the measurement of D in Fig. 1(d). Three important features are observed. First, D increases steadily as V_{qpc} becomes more negative. Second, the slope of D becomes larger immediately beyond pinch-off of the QPC ($V_{\text{qpc}} \leq -0.95$ V). Third, each steep rise in the QPC conductance is accompanied by a slight dip in D , indicated with dashed lines in Fig. 1(d).

These features may be qualitatively understood as follows. The first and second features are caused by the reduction in screening of V_{qpc} by the 2DEG, as V_{qpc} is made more negative and pushes the 2DEG away from the QPC. This recession becomes more rapid after pinch-off. The explanation of the dips associated with the opening of each mode is less straightforward. Intuitively, the divergence of the 1D density of states (1DOS) of the electrons in the QPC at the entry of each additional subband should be accompanied by an enhancement of the screening and a dip in D . Less obviously, enhanced screening at pinch-off could also result from the exchange interaction between conduction electrons.

To understand the features in D both qualitatively and quantitatively, we first simulate the device numerically,

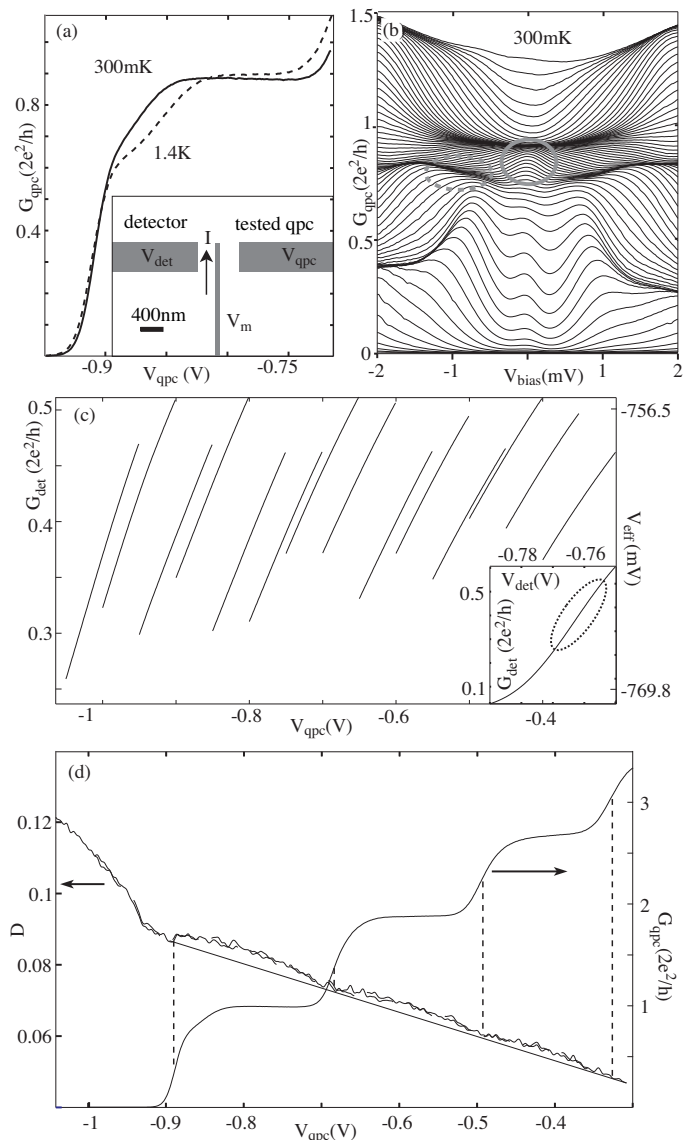


Figure 1: Linear (a) and non-linear (b) conductance of the device sketched in inset of (a). Plateaux fall below G_0 due to finite series resistance, not subtracted off in figures. Characteristic signatures [9] of 0.7 structure are observed: high-bias plateau near $0.8(2e^2/h)$ (dashed ellipse) and zero-bias anomaly (solid ellipse). c) Inset: Conductance of the detector QPC, used to derive the mapping $V_{\text{eff}}(V_{\text{qpc}})$. Optimal working range of the detector indicated by dotted ellipse. Main panel: 14 charge sensing measurements covering wide range of V_{qpc} . Left axis: detector conductance G_{det} . Right axis: V_{eff} mapped from V_{qpc} as described in text. d) Conductance trace of the QPC (right axis) and derivative $D \equiv dV_{\text{eff}}/dV_{\text{qpc}}$ of the detector data (left axis) for identical gate settings. D is a measure of screening of electric fields by the QPC. Dashed lines mark steep rises in the conductance of the QPC, coinciding with suppressions in D which indicate enhanced screening.

using M. Stopa's SETE code [18]. The simulation calculates self-consistently the effective potential and the

density in the QPC as a function of voltages on the electrostatic top gates, but does not include quantum corrections associated with the 1D constriction in the QPC [19]. Inputs to the simulation include the 2DEG growth parameters, geometry and voltages of the three gates, and temperature. The potential landscape of the device is calculated for a range of settings of V_{qpc} and V_{det} .

In Fig. 2(a) we plot D^{SETE} extracted from the simulated data using a procedure analogous to that described for D above. The quantitative match between the simulated D^{SETE} and the measured D is striking. In the simulation, as in the measurement, the kink in D^{SETE} occurs exactly at pinch-off [20]. This confirms the association of the change in slope with an electrostatic effect of emptying the point contact's saddle potential.

Both the measured and the simulated derivatives are linear above and below the kink at pinch-off. As seen in Fig. 2(a), the simulation is closely approximated by two lines intersecting at the pinch-off voltage. Fig. 2(b) has analogous lines to approximate the data above and below pinch-off and hence to emphasize the fact that the data drop below these guide lines at the transitions between conductance plateaux. The absence of such dips in the simulation, which includes only the classical electrostatic effect of the gates on the 2DEG, supports the argument that the modulations are caused by quantum mechanical effects such as a nontrivial 1DOS or exchange interaction.

The data in Fig. 2(b) show a pronounced dip at pinch-off. Understanding the source of this dip and the smaller dips associated with opening of successive subbands requires a quantum mechanical calculation. Since such a calculation of the full three dimensional system is very demanding, we perform a density functional theory (DFT) simulation of a device in which the QPC is modeled by a constriction in a long quantum wire that is wide enough to carry four spin-degenerate modes [21, 22]. In the inset of Fig. 2(c), the quantum wire is defined by gates marked V_c and the constriction by gates marked V_{qpc} . We further modify the dimensions and electron density to make the computation feasible. The width and the length of the simulated QPC are 250 nm and 200 nm, respectively, and the 2DEG is 70 nm below the surface. The donor density is 10^{11} cm^{-2} . The screened potential $V_{\text{det}2}$ is detected 200 nm beneath the center of the QPC. We simulate the device for a range of V_{qpc} such that the QPC has from zero to three open subbands – the thin solid line in Fig. 2(c) shows the conductance. Screening of V_{qpc} by the QPC affects the value of $D^{\text{DFT}} \equiv dV_{\text{det}2}/dV_{\text{qpc}}$. We use the local density approximation (LDA) for the exchange-correlation energy of the electrons in the 2DEG, using the known effective mass and dielectric constant for GaAs. Because of the modified geometry and the different electron density the DFT simulation cannot reproduce our measured D quantitatively. However the simulation clearly shows a dip whenever a new subband opens. In agreement with the measured data, the dip

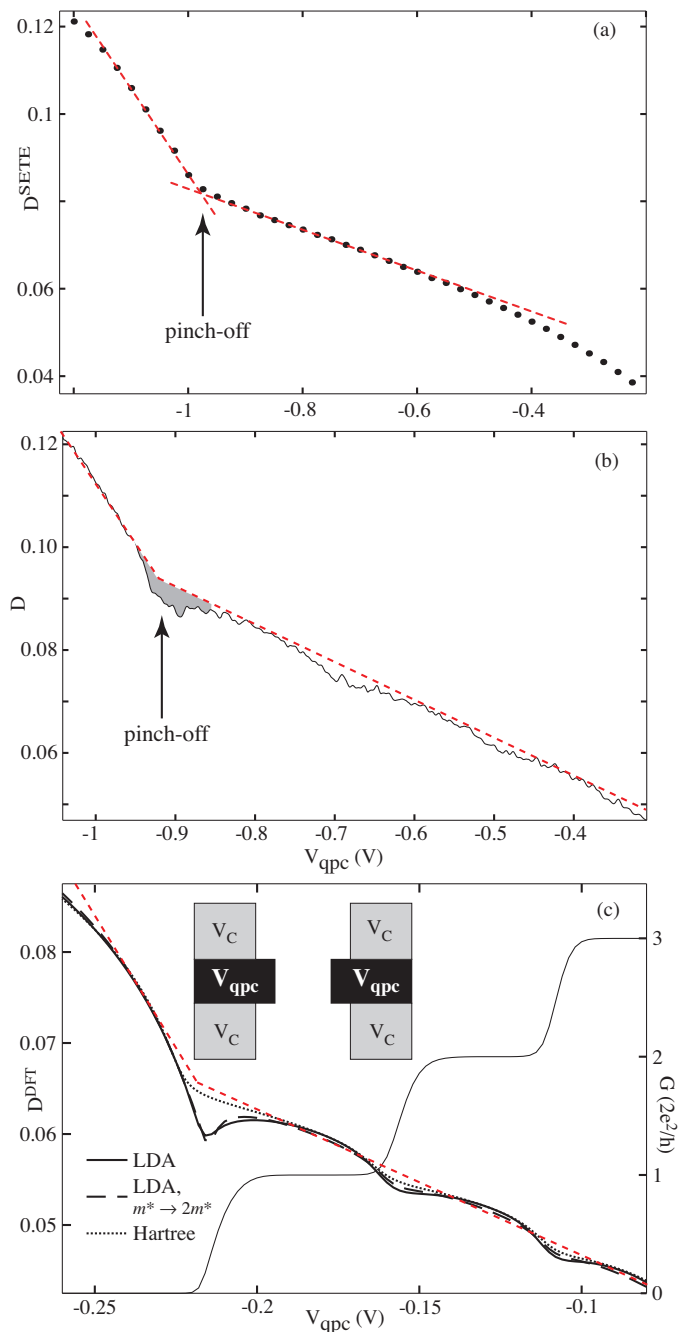


Figure 2: a) $D^{\text{SETE}} \equiv dV_{\text{eff}}/dV_{\text{qpc}}$ extracted from numerical simulation of the device. The red dashed lines are guides to the eye, showing linearity of D^{SETE} around pinch-off. No modulation can be observed in the simulation, which does not account for the one-dimensional nature of the QPC [19]. b) The shaded area indicates a pronounced dip of D around pinch-off. No such feature is observed in the simulated D^{SETE} . c) D^{DFT} , as calculated from DFT simulation of a modified QPC (inset) with a detector 200 nm beneath the plane of the QPC. Thick solid line: LDA with actual GaAs effective mass; dashed line: LDA with doubled mass; dotted line: Hartree approximation with actual mass. The thin solid line shows the conductance of the QPC in the LDA approximation (right-hand scale). The dashed red line is again a guide to the eye, showing the change in slope of the detector signal at pinch-off within all these simulations. The simulations dip below this guide line at the opening of each new mode. Within the Hartree approximation the dips are all roughly equal in size, but in LDA the dip at pinch-off is substantially larger than the others, as observed in experiment.

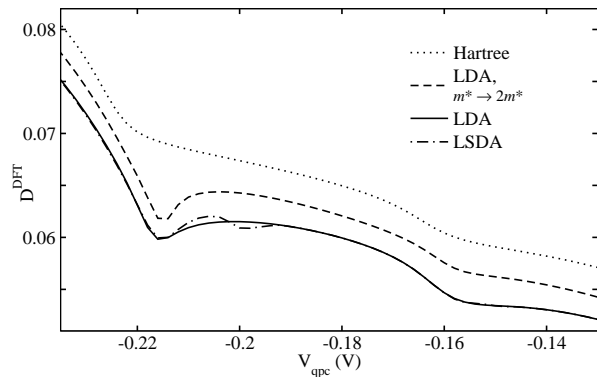


Figure 3: Curves from Fig. 2(c) expanded and shifted vertically to highlight subtle differences among the approximations at the opening of the first and second subbands. The LSDA curve with an additional dip associated with spin rearrangement is also shown, unshifted with respect to the LDA curve.

at the opening of the first subband is more pronounced than those for the second and third subbands. To estimate the importance of exchange and correlation we eliminate them by making the Hartree approximation (dotted curve) [23]. The dips are much weaker in this approximation (they disappear entirely in the Thomas-Fermi approximation) and all dips are of similar size, demonstrating that the larger dip at pinch-off in the LDA calculation is dominated by exchange-correlation effects. This is not surprising, since the exchange-correlation contribution to total energy at low carrier density is larger than the kinetic contribution: for quasi-1D systems, these two contributions go as $n^{3/2}$ and n^3 , respectively, where n is the linear density of electrons. The prominence of the dip at pinch-off relative to those for higher modes in the experiment (Fig. 2(b)) is thus evidence of the importance of exchange-correlation effects to charge distribution in a QPC. For higher modes, kinetic energy plays an important role: lowering kinetic energy by doubling effective mass (dashed curve, Fig. 2(c)) reduces dip area by 40%.

To see whether spin rearrangement within the QPC should be detectable by our compressibility measurements, we have also performed a DFT simulation using the local spin density approximations (LSDA) in which the density of electrons with spin up is not restricted to be the same as that for spin down. In this case the simulated detector signal has an additional small dip (Fig. 3, dot-dashed), marking the subtle rearrangement of electron density associated with the formation of a quasibound state at the center of the QPC. This smaller dip would be a signature of the formation of a magnetic moment responsible for the Kondo effect. Only one broad dip is discernible in the experimental data, precluding a clear experimental statement about spin rearrangement.

In conclusion, we have used a charge-sensitive detector to measure the charge rearrangement in a QPC as

it passes through pinch-off. The broad features in the detector signal closely match the predictions of a classical electrostatic simulation of the device. However, the charge redistribution at the entry of 1D subbands creates a series of dips in the detector signal. DFT calculations provide a good qualitative match to measurement, and indicate that the first dip is dominated by exchange interaction between electrons. The other dips are associated with the divergence of the density of states at the opening of each subband. Similar DFT calculations which further allow for the formation of local (spin-degenerate) magnetic polarization serve as the basis for the local moment Kondo scenario for 0.7 structure [9]. Our measurements are consistent with both LDA and these LSDA calculations, since in the calculations the spin rearrangement is accompanied by only a slight charge rearrangement.

We thank the NNIN Computation Project for SETE, and L. P. Kouwenhoven and L. H. Willems van Beveren for computer access. Work at Stanford was supported by contracts from the US AFOSR (F49620-02-1-0383) and the US ONR (YIP, N00014-01-1-0569). Work at BGU was supported by the BSF. SL acknowledges a SNF Fellowship, DGG support from the Sloan Foundation and Research Corporation, and TR support from the Kreitman Foundation. During the review process, we became aware of related work on carbon nanotubes [24].

Supplementary Information: Results of the DFT calculation with the potential detected in the 2DEG plane

In the DFT calculation we unfortunately cannot simulate a device in which both the measured QPC and the detector QPC are present. In order to perform such a calculation we would have to put both QPCs inside a very wide quantum wire. The number of modes such a wire would have to support would be too large for the calculation to be feasible. In the single QPC geometry we used in our DFT calculation we could have measured the potential in the 2DEG plane next to the QPC instead of 200 nm below the 2DEG plane as we did. It turns out that the features observed in the experiment and in our DFT calculation can also be observed if we simulate measuring the potential in the 2DEG plane (see Figure S1.) In Figure S2, the derivative D was calculated from the potential measured in the 2DEG plane 300 nm from the center of the QPC. As in the calculation presented in the paper, there is a large dip at pinch-off and a series of weaker dips corresponding to higher transverse modes being occupied in the QPC. Observation of these features in two different geometries supports our contention that they are qualitatively linked to the features we observe in the experiment. However, because the experimental geometry is different from that of the two calculations we cannot claim that the calculations should quantitatively account for the magnitudes of the dips in the real device.

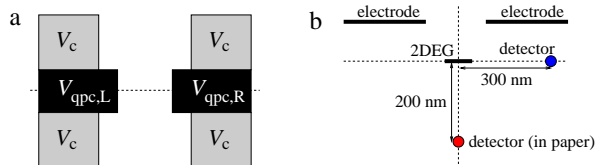


Figure S1: a) The electrodes of the modified QPC used in the DFT calculation. b) The cross section through the center of the QPC (dashed line in panel a). The red dot 200 nm below the 2DEG is the position of the detector in the calculation presented in the paper. The derivative D^{DFT} calculated from the potential in the 2DEG plane 300 nm from the center of the QPC (blue dot) is shown in the next figure. In the calculation presented in the paper the voltages on both gate electrodes were changed together ($V_{\text{qpc,L}} = V_{\text{qpc,R}}$), while in the present calculation $V_{\text{qpc,R}}$ was fixed and we only varied $V_{\text{qpc,L}}$.

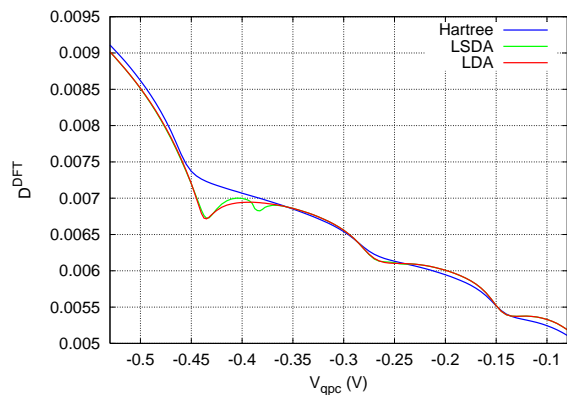


Figure S2: The derivative D^{DFT} calculated from the potential off to the side in the 2DEG plane (detector location is shown as a blue dot in Fig. S1b). The curves for three different approximations are shown: DFT within local density approximation (red), DFT within local spin-density approximation (green) and the Hartree approximation (blue). The curves show very similar behavior to that of the calculation presented in the paper (Fig. 2c and Fig. 3), showing that the detailed geometry is not important in determining the qualitative features of the compressibility measurement, as long as the system under study lies between the gate that is varied and the detector. The magnitude of D^{DFT} , however, is smaller here because the right gate electrode effectively screens the potential. In the experiment, the electrode separating the two QPCs is very thin and is thus less effective in screening the potential.

Adjustable parameters

We did not adjust parameters to try to achieve the best possible fit to the data. Rather, we chose values for parameters as close as possible to the values in the real device while maintaining computational feasibility.

Values for most of the important parameters for the DFT calculation are given in the manuscript. Other relevant parameters are the lithographic width of the quantum wire away from the QPC (300 nm), the voltage on the quantum wire electrodes ($V_c = -0.08$ V) and the position of the donor layer (20 nm below the surface). The details of our numerical approach are presented in a separate publication [21].

Can spin rearrangement be detected with our method?

The additional dip near pinch-off in the local spin-density approximation (LSDA) calculation is related to formation of a spin-1/2 magnetic moment in the QPC. Somewhere between pinch-off and the transition to the first conductance plateau, a quasibound state forms at the center of the QPC just below the Fermi energy. The quasibound state can be occupied with either a spin-up or a spin-down electron, i.e. the QPC acts as a spin-1/2 magnetic moment. The formation of the magnetic moment is accompanied by a slight rearrangement of the electron density within the QPC, which shows up as an additional dip in D .

As alluded to above, some of the present authors have performed an extensive study of the conditions under which such a magnetic moment forms in the QPC [21]. We observed this feature only in the DFT calculation within the local spin-density approximation. In the ordinary local density approximation the two spin-densities are restricted to be the same and thus spin-polarization in the QPC is not possible, while in the Hartree approximation the exchange interaction, which is responsible for spin-polarization, is absent. We observed the formation of the magnetic moment for various geometries of the QPC (rectangular shape of QPC electrodes or more adiabatic, triangular shaped electrodes) and for a wide range of QPC widths and 2DEG densities. The parameter which affects the formation of the quasibound state in the most important way is the length of the QPC. For a substantial range of QPC lengths the situation is the same as presented in this paper. However, if the QPC is very short there is not enough space for the quasibound state to form in it. If the QPC is very long an antiferromagnetically ordered spin chain forms instead of a single spin-1/2 magnetic moment.

Our present experiment cannot resolve the extra dip described by the LSDA calculation, but future, more sen-

sitive measurements may be able to detect it.

-
- [1] K. J. Thomas et al., Phys. Rev. Lett. **77**, 135 (1996)
 - [2] R. de Picciotto et al., Phys. Rev. Lett. **92**, 036805 (2004)
 - [3] C.-K. Wang et al., Phys. Rev. B **57**, 4552 (1998)
 - [4] B. Spivak and F. Zhou, Phys. Rev. B **61**, 16730 (2000)
 - [5] H. Bruus et al., Physica E **10**, 97 (2001)
 - [6] K. A. Matveev, Phys. Rev. B, **70**, 245319 (2004)
 - [7] Y. Meir et al., Phys. Rev. Lett. **89**, 196802 (2002)
 - [8] K. Hirose et al., Phys. Rev. Lett. **90**, 026804 (2003)
 - [9] S.M. Cronenwett et al., Phys. Rev. Lett. **88**, 226805(2002)
 - [10] J. Eisenstein et al., Phys. Rev. Lett. **68**, 674 (1992)
 - [11] S. Shapira et al., Phys. Rev. Lett. **77**, 3181 (1996)
 - [12] S. Ilani et al., Nature **427**, 328 (2004)
 - [13] M. Field et al., Phys. Rev. Lett. **70**, 1311 (1993)
 - [14] D. Sprinzak et al., Phys. Rev. Lett. **88**, 176805 (2002)
 - [15] J. M. Elzerman et al., Appl. Phys. Lett. **84**, 4617 (2004)
 - [16] I. M. Castleton et al., Physica B **249**, 157 (1998)
 - [17] A. Kristensen et al., Phys. Rev. B **62**, 10950 (2000)
 - [18] M. Stopa, Phys. Rev. B **54**, 13767 (1996)
 - [19] The simulation solves Schrödinger and Poisson equations in the growth direction at each point on a grid in the plane of the 2DEG. Then it calculates the density self-consistently using a Thomas-Fermi approximation.
 - [20] Pinch-off in the simulation is defined as the point where the conduction band edge is equal to the Fermi energy exactly at the saddle point.
 - [21] T. Rejec and Yigal Meir, Nature **442**, 900 (2006)
 - [22] See EPAPS Document No. E-PRLTAO-98-033719 for discussion of our DFT calculation. For more information on EPAPS, see <http://www.aip.org/pubservs/epaps.html>. This Supplementary Info is included at the end of the present version, posted on the cond-mat archive.
 - [23] The exclusion of exchange and correlation affects the density far away from the QPC. To partly compensate for this effect we shifted the Hartree curve so that it matches the DFT result far beyond pinch-off.
 - [24] S. Ilani et al., Nature Phys. **2**, 687 (2006)